GIMBALLING MAGNETIC BEARING REACTION WHEEL WITH DIGITAL CONTROLLER

Bernd Gerlach[(1)], Markus Ehinger[(1)], Hans Knut Raue[(1)], René Seiler[(2)]

[(1)] TELDIX GmbH, Heidelberg, 69123, Germany, Email: Gerlach@teldix.de
[(2)] ESA/ESTEC, Noordwijk ZH, 2200 AG, The Netherlands, Email: Rene.Seiler@esa.int

ABSTRACT

Magnetic bearing reaction wheels provide a number of interesting advantages over ball bearing wheels. They allow high-speed operation with minimum loss torque and generate substantially less micro-vibrations. However, they require dedicated, demanding control electronics. A controller based on a Digital Signal Processor has been developed. The controller was tested with an 87 Nms wheel prototype equipped with a magnetic bearing allowing active control in five axes. The wheel provides low-noise operation from 0 to 8000 rpm with a rotor gimballing capability of up to ±1.7°. The paper reviews the design principles and presents relevant test results, e.g. regarding the active suppression of micro-vibrations.

1. INTRODUCTION

Magnetic bearing reaction wheels (MBRW) may be operated at higher speeds, thus improving the momentum-to-mass ratio, and may be designed to reduce the micro-vibration signature compared to ball bearing momentum and reaction wheels. MBRW's show a low mean loss torque and do not exhibit loss torque fluctuations due to oil distribution changes over time or temperature. No special care has to be taken to guarantee lubrication over a wide range of operating conditions. Neither high speed operation nor frequent zero crossings affect the lifetime of the contact-less magnetic bearing. It is free of both stiction effects and high loss torque variations around zero rpm. Neither evacuation nor hermetical sealing is necessary.

A magnetic bearing wheel with five actively controlled axes provides an additional significant advantage: the spin axis is positioned by electronic bearing control. The flywheel can be allowed to rotate freely around its natural spin axis, i.e. its principal axis of inertia. The orientation of this axis with respect to the mounting interface may be adjusted by the electronics thus reducing the balancing effort for the rotor. In addition, gimballing of the flywheel is possible to some extend and in this manner a fine pointing capability is provided. All three spacecraft axes may be controlled by just one wheel. In some cases, this allows the reduction of the number of wheels on a spacecraft from three plus one spare to just one plus one spare.

There are some disadvantages associated with the magnetic bearing concept. One is the increased complexity of the wheel. Position sensors, controller and powerful actuators are needed. Fortunately, the permanent magnets of the actuators increase the rotating mass and provide additional momentum. Due to the additional sensors, electronics and actuators as well as the necessary emergency ball bearings, the mass of the wheel is higher in comparison with a ball bearing wheel. However, the additional mass can be partially compensated by reducing the rotor diameter, benefiting from a much higher rotational speed.

High-speed operation and the controller electronics require additional power, while the expected in-orbit power consumption of the bearing is low. A portion of the additional power consumption can be compensated by the lower loss torque of the bearing that results in reduced steady-state motor power consumption. The overall power consumption, nevertheless, is higher than for a ball bearing wheel. On the other hand, this power consumption should be compared with the steady-state power consumption of three conventional wheels under worst-case friction conditions.

Another disadvantage of the magnetic bearing wheel leading to additional mass is the need for a rotor locking mechanism to sustain the launch loads.

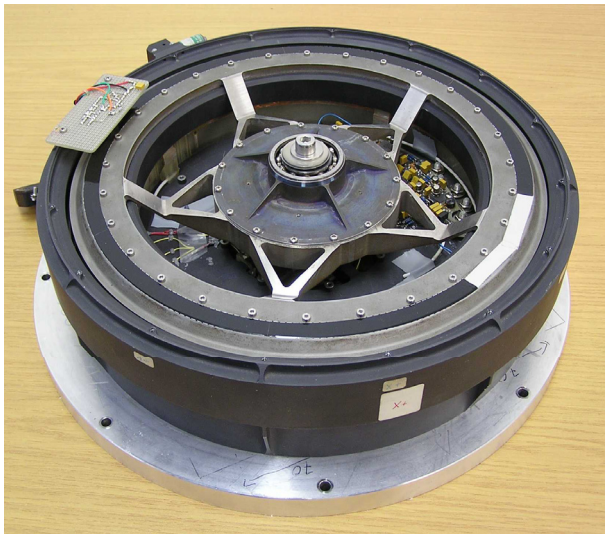

Fig. 1. Five Axes Magnetic Bearing Reaction Wheel

2. FUNCTIONAL DESCRIPTION

The wheel hardware is based on an Engineering Model design (Fig. 1) originally developed for use in conjunction with analogue control electronics. Most analogue control and power electronics have now been removed. Only the original sensor drive electronics is still in use. The new digital electronics (not shown) is located outside of the wheel.
The magnetic bearing gap width is ±1 mm in X, Y and ±0.5 mm in Z direction. Table 1 summarizes the main technical characteristics of the wheel.

Nominal Speed [rpm]	6000	8000
Angular Momentum [Nms]	65.6	87.5
Transverse Momentum [Nms]	1.95	2.6
Usable Gimballing Angle [deg]	1.7	
Max. Motor Torque [Nm]	0.25	
Max Gimbal Torque [Nm]	0.6	
Total Weight [kg]	11.85	
Height [mm]	109	
Diameter [mm]	343	
Steady-State Power [W]	18	25
Max Power [W]	140	

Table 1. Key Technical Characteristics

2.1 Sensors

Inductive position sensors are applied for each of the five degrees of freedom. Each sensor contains multiple coils allowing compensation of noise effects. The resolution is better than 1µm. The sensors provide continuous position signals. However, these signals are neither linear nor independent from each other. They require linearization before use as controller input.

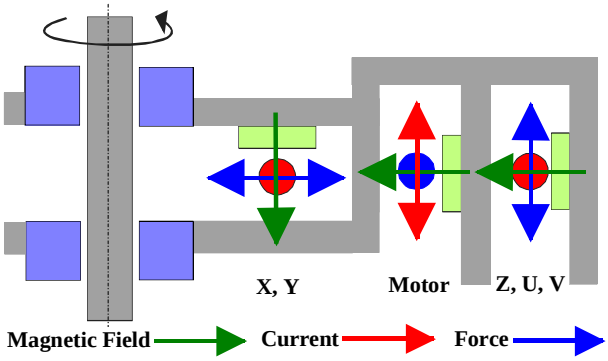

Fig. 2. Sectional view of the rotor: Force generation by the bearing actuators

2.2 Actuators

The magnetic bearing (Fig. 2) operates on the electro-dynamic principle much like a brushless DC motor. Permanent magnets provide a magnetic field. Actuator coils are mounted perpendicular to the magnetic field. Current through the actuator coils generates a force perpendicular to both the current and to the magnetic field. There is a linear relation between current and force. In case no current is applied, no force will be generated. This principle allows in-orbit low power operation.

There are individual actuator coils for each of the X and Y axes. The actuator for the Z direction is divided into four coils. Simultaneous control of all four coils generates forces in Z direction, individual control generates torque either in U (around the X axis) and V (around the Y axis) directions, respectively.

An additional levitation coil is used to compensate for gravity on ground, limiting the operation of the MBRW to one fixed orientation for ground testing.

2.3 Motor

The MBRW is driven by a three-phase brushless DC-motor with fourteen pole pairs. The motor design is similar to those used in standard ball bearing wheels. Thus, standardized wheel drive electronics (WDE) may be used. The maximum motor torque and power consumption depends on the selected WDE. The data on power consumption presented in Table 1 are based on measurements with a previously used analogue controller. The digital controlled MBRW has been operated in an environment evacuated down to only 15 mbar, which is not representative of the space environment and does not provide realistic power measurements for in-orbit operation. Hence, the in-orbit power consumption should be substantially lower.

3. WHEEL ELECTRONICS

Goal of the first phase of the MBRW design project was the development of the control algorithms. Therefore, standard electronic components were used.

Fig. 3 shows a block diagram of the wheel electronics. The wheel contains the inductive position sensors, the sensor drive electronics, actuator coils, the levitation coil for the magnetic bearings, the three-phase motor coils as well as the Hall-effect sensors for the motor. A set of temperature sensors provides information on individual coil temperatures.

Outside the wheel, there are three additional boxes (shown in yellow) for the controller, the actuator PWM amplifiers and the wheel drive electronics (WDE). The controller box contains two boards, a commercial DSP evaluation board and an interface circuit board. The actuator amplifier box contains four boards with PWM power amplifiers to drive the actuator coils. The third box contains a standard WDE. The WDE is nearly identical to the WDE of a conventional ball bearing wheel. The only modification has been that the speed limiter was disabled. The WDE is controlled by the DSP and the associated interface signals are generated by the DSP as well.

The Ground Support Equipment (GSE) is based on a standard PC and operates with the IDA GSEOS 5.24 software [1]. It communicates with the DSP over a CAN-bus.

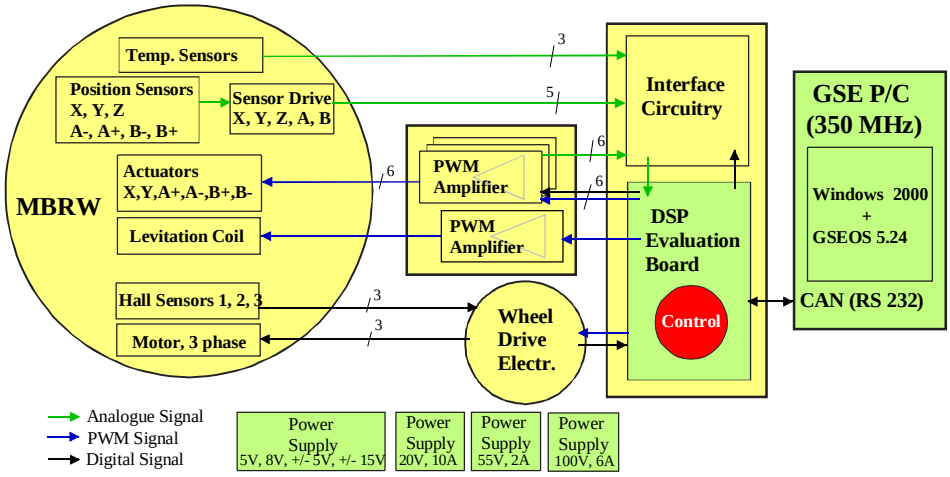

Fig. 3. Block diagram of the wheel electronics

4. DIGITAL CONTROLLER

The digital controller is based on a 160 MHz 16 bit fix-point DSP and provides a maximum of flexibility. All parameters may be changed by telecommand. Therefore, in-orbit reconfiguration is possible. Also, it provides a wide range of high-resolution housekeeping data.

The instantaneous rotor position is measured by inductive sensors with a resolution of better than 1µm. The sensor drive electronics converts the sensor data into five analogue voltages for X, Y, Z, A and B raw positions. A and B are tilt angles turned by 45° with respect to the U (around X) and V (around Y) axis, respectively.

The raw positions are digitized and linearized by the DSP. This step requires extensive computing. Each position component depends on all five raw position components. Therefore, a full 5 x 5 matrix with polynomials up to the power of five has to be used to express the relationship between sensor voltages and position. Also, the rotor displacement speed is calculated. Both position and speed are filtered for noise reduction. The controller is based on a PID controller for each axis. Some control parameters are speed dependent and have to be adapted to the rotor speed. The controller computes the forces (X, Y and Z) and torques (U and V) for the magnetic bearing. The forces and torques are converted into the required actuator currents for the six actuator coils (X, Y, A+, A-, B+ and B-). Then, the currents are converted into pulse width modulation (PWM) ratios. The PWM signals are generated by the DSP and amplified. Finally, the currents sent through the actuator coils produce the forces required to adjust both the rotor position and orientation.

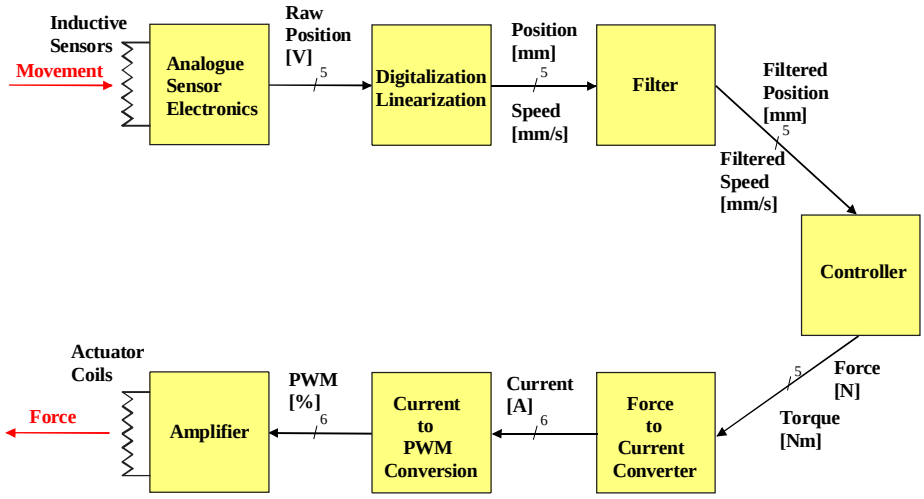

Fig. 4. Digital Controller

4.1 Wheel Operation

Fig. 5 shows a typical data plot as displayed by the GSE. It presents the Y-position of the wheel at 0 rpm as a yellow colored area sampled over a time period of one second. The diagram is divided into three sections with different resolutions. The upper section (light gray background) covers the range from the maximum gap width (+1.0 mm) to +0.1 mm. The middle section has a dark gray background and shows an enlarged area from +0.1 to –0.1 mm. The lower section covers the area from –0.1 to –1.0 mm. The position of the free flying rotor is controlled with an accuracy of ±10 µm with respect to the commanded position.

Fig. 6 shows a time window with the width of one second for the Y-position at 3000 rpm. Static imbalance and magnetic variations force the rotor to spin around the centre of mass. Since it is generally not identical to the geometrical centre a position change of about ±30 µm can be seen for each revolution. Fig. 7 shows the same signal for a rotor speed of 8000 rpm. The interference pattern is caused by the limited display resolution.

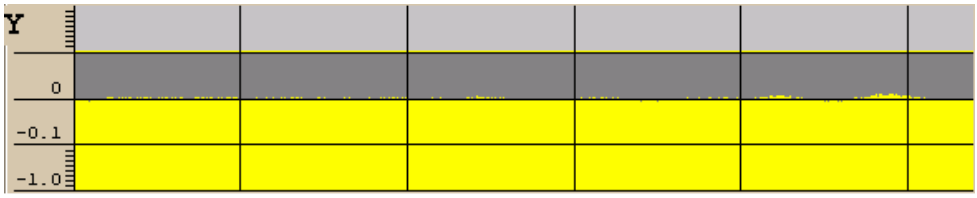

Fig. 5. Y-Position in mm at 0 rpm over 1 second

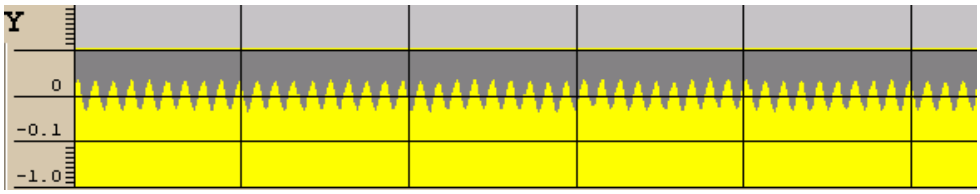

Fig. 6. Y-Position in mm at 3000 rpm over 1 second

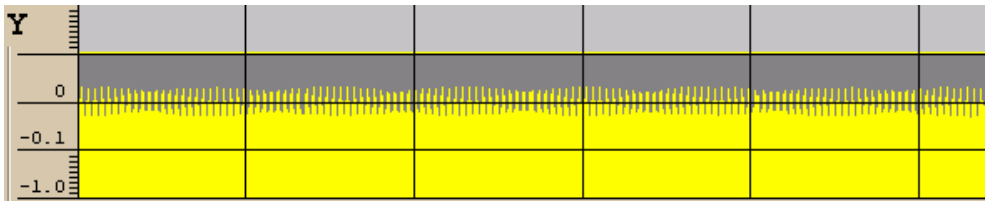

Fig. 7. Y-Position in mm at 8000 rpm over 1 second

5. FILTER

Static and dynamic imbalance as well as magnetic variations causing a rotor displacement depending on the rotor speed. For position control of the rotor, only its centre position is of importance. To keep the rotor in this centre position, the cyclic position changes due to the rotation have to be filtered in order to avoid unnecessary corrective actions of the control loop generating unwanted microvibrations within the spacecraft. Standard filters slow down the response times against external disturbances. This would reduce the overall performance of the wheel. Therefore, a self-learning filter algorithm has been developed. The filter tolerates the displacement caused by both static and dynamic imbalance without applying compensation forces, and therefore avoiding negative effects on the loop stability.

The algorithm compensates signals up to the first seven harmonics of the rotor speed. Due to this filter, the rotor is allowed to spin around its natural spin axis, i.e. principal axis of inertia, identical to its centre of mass without additional balancing and without generating micro-vibration signatures typically known from ball bearing reaction wheels. Fig. 8 shows the force in Y-direction at 4000 rpm with active filters and after filter reset.

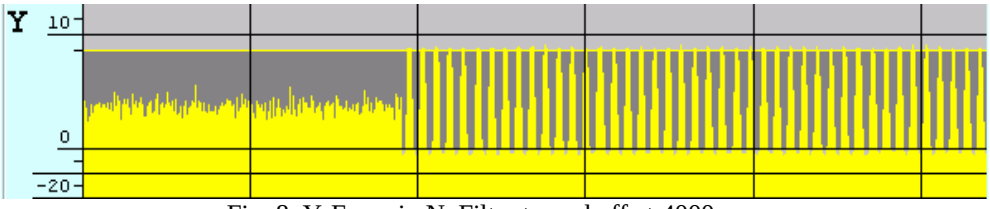

Fig. 8. Y-Force in N, Filter turned off at 4000 rpm

6.1 Micro-Vibrations

To verify the expected improvements on the micro-vibration signature, some first measurements were performed. These measurements were done without having optimized equipment available. The wheel was located in a small vacuum chamber at ~15 mbar connected to a continuously operating vacuum pump. The vacuum chamber containing the wheel was mounted on top of the dynamometric platform. Also, the levitation coil was activated causing coupling effects between actuator coils.

Magnetic variations of the rotor magnets and asymmetric characteristics of the levitation coil cannot be compensated without external sensors. Unfortunately, the magnets in the X and Y actuators have magnetic properties that vary up to 14% between each other. It has to be assumed that the variation of the magnetic field of the magnets used to control the Z position is in the same order of magnitude. Thus, a static coil current in the X, Y or Z actuator and in the levitation coil generate fluctuating forces derived from the field inhomogenity produced by the varying characteristics of the magnets. This effect could not be compensated, but the disturbance forces transferred to the surrounding environment are proportional to the applied forces. Since the levitation coil has to support the mass of the rotor during on-ground operation, this effect should be much smaller in micro-gravity conditions.

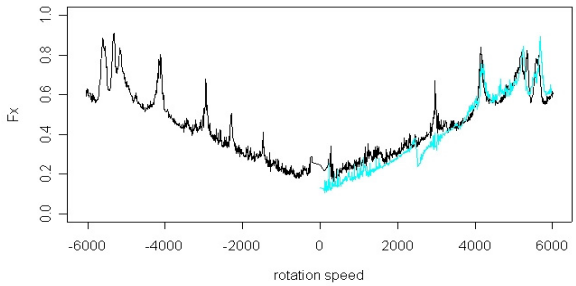

Fig. 9. X-force in N, Total Spectral Power from 2 to 500 Hz. Vacuum Pump on (black) / off (blue).

Fig. 9 shows the total spectral power for micro-vibrations from 2 to 500 Hz for forces in X-direction. The black line represents a speed profile from –6000 rpm to 6000 rpm with the vacuum pump on, whereas the blue line is a result of a speed profile from 6000 rpm down to 0 with the pump switched off. The values around zero rpm are not valid because of imperfections of the measurement equipment.

Fig. 10 and 11 show the total spectral power of microvibrations in N from 2 to 500 Hz for forces in radial (X) and axial (Z) direction respectively and speeds from –6000 rpm to 0 rpm either with filters on (black) and off (red). It can be clearly seen that the low noise operation mode effectively reduces the microvibration forces up to a factor of 4. This is equivalent to a fine balancing of the wheel. Fig. 12 shows the total spectral power of microvibration torque in Nm around the X-Axis (U-Axis). Again the low noise operation mode is able to reduce the torque by up to factor 4.

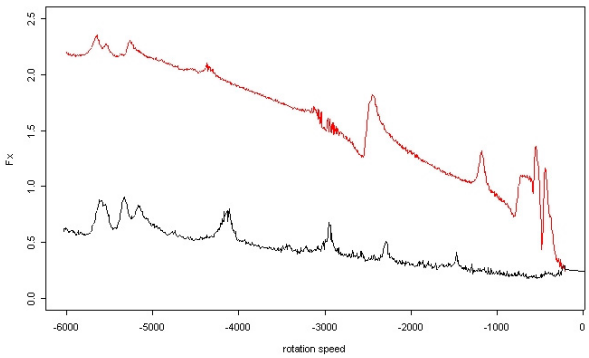

Fig. 10. X-force in N, Total Spectral Power from 2 to 500 Hz, Filter on (black) / off (red).

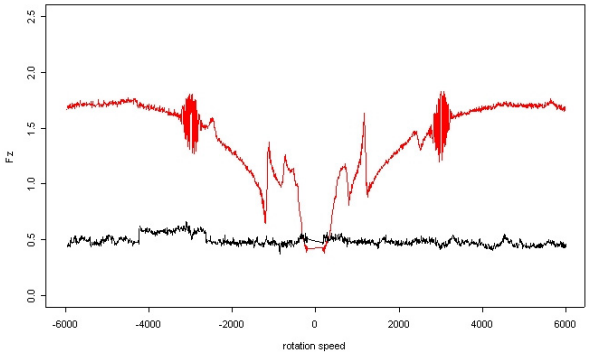

Fig. 11. Z-force in N, Total Spectral Power from 2 to 500 Hz, Filter on (black) / off (red).

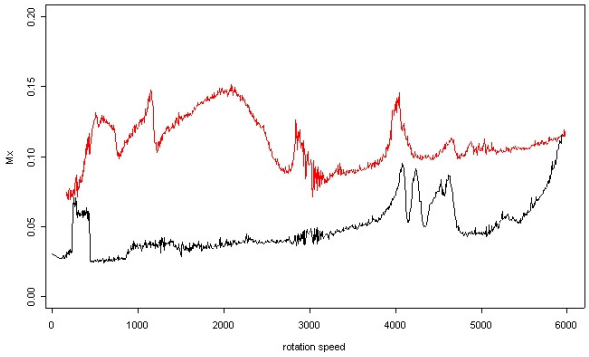

Fig. 12. U-torque in Nm, Total Spectral Power from 2 to 500 Hz, Filter on (black) / off (red).

Even in this non-optimal test environment, the MBRW demonstrated a better micro-vibration performance compared to conventional ball bearing

wheels with similar rotating mass. Much better results are to be expected without the adverse effects of the levitation coil, vacuum pump and vacuum chamber.

6. VIBRATION SUSCEPTIBILITY TESTS

Vibration tests with in-orbit levels (table 2) have been performed to demonstrate the robustness of the controller against external disturbances. Sine vibrations have been applied in both X and Z-directions for various speeds up to 3000 rpm. During random vibrations, the speed was changed from 0 to +/- 3000 rpm. Furthermore, the rotor was tilted up to 1.0°.

f [Hz]	G
5 - 200	10^{-2}
200 - 450	Decrease based on $1/f^2$
450 - 2000	$3 \bullet 10^{-3}$

Table 2. Typical In-Orbit Vibration Levels.

Fig. 13 shows a GSE screenshot of X and Y position over one second during 3000 rpm and random vibrations of 0.5 G rms in X-Axis direction.

Fig. 14 shows a GSE screenshot of Z data over one second during 3000 rpm and tilt angle (U-direction) of 1.0° at 0.3 G rms random vibrations in Z-axis.

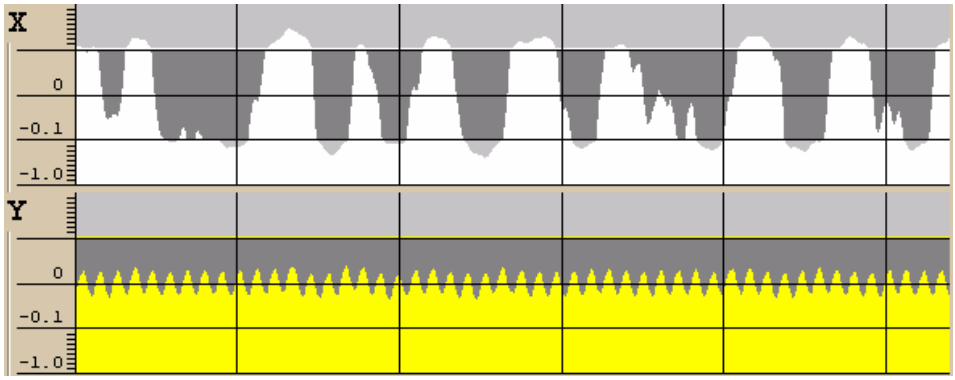

Fig. 13. X and Y-position in mm, at 3000 rpm, 0.5 G rms random vibrations in X-direction. Middle section with dark gray background enlarged.

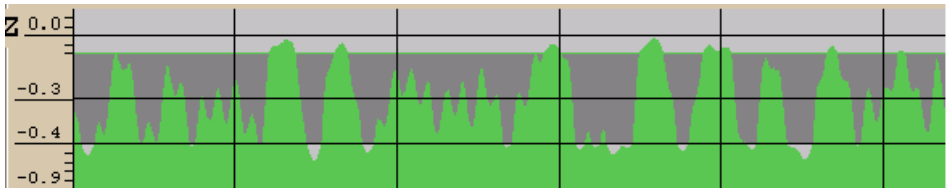

Fig. 14. Z-position in mm, at 3000 rpm, 0.3G rms random vibrations in Z-direction. Middle section with dark gray background enlarged.

RESUME

It has been demonstrated that a digital controller is able to provide stable operation of a five axes magnetic bearing and provides an increased performance over analogue controllers in low noise mode with still robust rotor position control even at 0.3 G rms random vibration in axial or radial direction. The performance of a five axes magnetic bearing wheel turns out to be effectively limited by the mechanics of the actuators and the tolerances of the magnets and no longer by the control electronics. With the new digital controller, much of the electronics complexity and high precision requirements could be moved from hardware into more flexible software algorithms.

ACKNOWLEDGEMENTS

B. Gerlach thanks both ESA and DLR for their support of the magnetic bearing wheel development. The project was funded by ESA Contract No. 10.977/94/NL/PP and supported by DLR contributions Ref. No. 50TT9717. B. Gerlach thanks Mr. Siegfried Häußler, Mr. Dieter Layer, Mr. Joachim Mohr and Dr. Sebastian Schlicht for their support during the project.

REFERENCES

1. K. Stöckner, IDA GSEOS V homepage http://www.gseos.de/